Scilight

Smart Chemical Engineering

https://www.sciltp.com/journals/sce

Article

Check for updates

Data-Driven Condition-Aware Adaptive Model Predictive Control for Industrial Ethylene Cracking Furnaces

Mengjie Luo [1], Mengxuan Zhang [2], Yunpeng Zhao [1], Xiaogang Shi [1] and Xingying Lan [1,*]

[1] State Key Laboratory of Heavy Oil Processing, China University of Petroleum-Beijing, Beijing 102249, China
[2] Jinglianwen Innovation Center for Digital Technology, Hangzhou 310000, China
* Correspondence: lanxy@cup.edu.cn; Tel.: +86-18610962527

How To Cite: Luo, M.; Zhang, M.; Zhao, Y.; et al. Data-Driven Condition-Aware Adaptive Model Predictive Control for Industrial Ethylene Cracking Furnaces. *Smart Chemical Engineering* **2026**, *2*(2), 5. https://doi.org/10.53941/sce.2026.100005

Received: 22 April 2026
Revised: 3 June 2026
Accepted: 11 June 2026
Published: 16 June 2026

Abstract: During long-term operation of ethylene cracking furnaces, coke deposition and operating condition variations continuously alter process dynamics, resulting in strong non-stationarity and reduced control performance of conventional model predictive control (MPC). To address this issue, a condition-aware adaptive MPC (CA-AMPC) framework is proposed, in which operating conditions are incorporated into the control loop to enable adaptive prediction and control adjustment. A segment-wise operating condition identification method combining change point detection and clustering is developed to capture both abrupt transitions and gradual process evolution. Based on the identified conditions, condition-dependent prediction models and optimized control parameters are dynamically activated to improve control adaptability under varying operating regimes. Industrial case studies demonstrate that the proposed framework achieves yield improvements of approximately 1.0%, 1.5%, and 0.3% under normal-load early-coking, normal-load severe-coking, and post-decoking high-load conditions, respectively. The total online computation time remains well below the 120 s DCS sampling interval. The proposed framework provides an effective solution for adaptive control of non-stationary industrial processes.

Keywords: operating condition identification; bayesian optimization; model predictive control; ethylene cracking; data-driven

1. Introduction

Ethylene is a fundamental feedstock in the petrochemical industry, and cracking furnaces serve as the primary production units that directly determine reaction efficiency and economic performance [1,2]. To meet increasing demands for energy efficiency and emission reduction, furnace operation must achieve high efficiency while maintaining long-term stability under varying conditions [3–5]. However, the ethylene cracking process involves complex interactions among chemical kinetics, heat transfer, and mass transfer, leading to strong nonlinearity, multivariable coupling, and pronounced non-stationarity [6,7]. These characteristics pose significant challenges for advanced control.

Conventional control strategies exhibit fundamental limitations under such conditions. Proportional-integral-derivative (PID) control, which is widely adopted in industrial practice, relies on single-loop feedback control and assumes operation near a steady state [8,9]. However, the cracking process exhibits strong spatial coupling and time-varying dynamics, making it difficult for PID to achieve coordinated multivariable regulation. In addition, long-term operation of ethylene cracking furnaces under harsh thermal and chemical environments leads to equipment-level deterioration, including corrosion, erosion-corrosion, and material degradation [10,11]. These phenomena further exacerbate process uncertainty and operational complexity. As a result, conservative tuning is often employed to ensure stability, which limits optimization potential and economic performance [12–14].

Model predictive control (MPC) provides a systematic framework for multivariable optimization and constraint handling, and has been widely applied in process industries [15–17]. Nevertheless, its performance critically depends on model accuracy and parameter settings. Conventional MPC typically utilizes a global model with pre-configured weighting parameters, which implicitly assumes stationary process dynamics. In practice, however, ethylene cracking furnaces exhibit continuous process evolution during long-term operation [18]. Coke deposition gradually alters heat-transfer efficiency and reaction kinetics, while variations in feed composition and operating load further change coupling relationships and system behavior [19,20]. As a result, the process operates across multiple regimes with distinct dynamic characteristics. Under such evolving conditions, fixed-model MPC suffers from persistent model mismatch, leading to degraded prediction accuracy and control performance, especially during regime transitions [21,22].

In recent years, data-driven and artificial intelligence approaches have been increasingly adopted for modeling, condition monitoring, and optimization of complex industrial processes [23–27]. Existing studies have explored clustering-based methods for operating condition identification [28–30] and advanced learning models for process prediction and control [31–34]. However, these efforts are typically developed in isolation. Operating condition identification, predictive modeling, and control design are often treated as separate tasks, without establishing a direct linkage between process evolution and control adaptation. Consequently, most existing control strategies still rely on a single model or loosely coupled multi-model schemes, which assume limited variation in operating conditions [35]. This assumption becomes invalid under significant regime transitions, resulting in reduced robustness and stability [36,37].

To overcome these limitations, it is essential to explicitly incorporate operating condition evolution into the control loop, enabling coordinated adjustment of both prediction and control layers. From this perspective, operating conditions should not be treated merely as descriptive labels, but as decision-driving variables that determine model selection and control configuration. This motivates the development of a unified condition-driven control framework for nonstationary industrial processes.

Therefore, this study proposes a condition-aware adaptive model predictive control (CA-AMPC) framework for ethylene cracking furnaces. A segment-wise operating condition identification method is developed to capture both abrupt transitions and gradual process drift. A condition-dependent predictive modeling approach is further established to represent heterogeneous dynamics under different operating regimes. Based on the identified conditions, both prediction models and optimally tuned control parameters are adaptively selected, enabling coordinated adjustment of prediction and control layers. A smooth switching mechanism is introduced to ensure stable transitions across operating regimes. The main contributions of this work are summarized as follows:

(1) A condition-driven control paradigm is established for nonstationary industrial processes, in which operating conditions are explicitly incorporated as decision-driving variables within the MPC framework.
(2) A segment-wise operating condition identification method is proposed to capture both abrupt transitions and gradual drift, providing a physically consistent representation of evolving operating regimes.
(3) A condition-dependent modeling and control strategy is developed, enabling coordinated adaptation of prediction models and control parameters under varying conditions.
(4) The proposed framework is validated on an industrial ethylene cracking furnace, demonstrating improved control performance and robustness.

2. Methodology

As illustrated in Figure 1, the proposed framework integrates operating condition identification, prediction of key process variables, and optimization-based control within a unified condition-driven architecture. The framework operates in two phases, namely offline and online. In the offline phase (Figure 1a), historical industrial data is used to identify operating conditions, train condition-specific prediction models, and optimize control parameters. In the online phase (Figure 1b), real-time data are processed through the condition identification module to determine the current operating condition. The corresponding prediction models and control parameters are then activated to enable adaptive optimization of the cracking process. The following sections present the implementation details of each module.

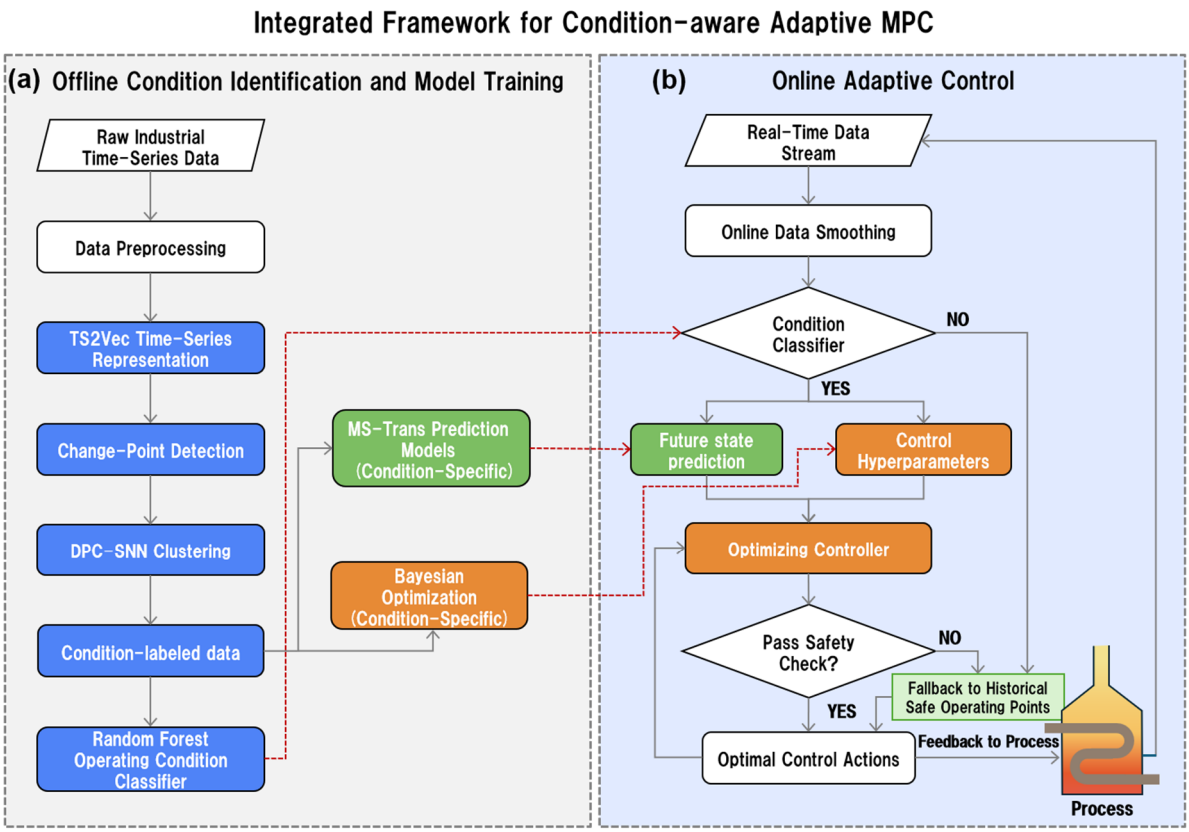

Figure 1. Schematic of the CA-AMPC framework: (**a**) offline phase for condition identification and model training. (**b**) online phase for real-time adaptive optimization and control.

2.1. Operating Condition Identification in CA-AMPC

The ethylene cracking process exhibits multi-timescale dynamics [38]. Manipulated variables evolve rapidly to drive operational transitions, while coke accumulation and catalyst variations evolve slowly over time [39,40]. These coupled fast-slow dynamics induce both discrete condition shifts and continuous state evolution, making it necessary to capture temporal evolution for reliable operating condition identification.

Conventional methods rely on static clustering of raw data. However, the i.i.d. assumption is inconsistent with the temporal dependencies in petrochemical process data [35,41,42]. Moreover, reliance on purely spatial distances may lead to misgrouping under process drift, where temporally distant but spatially similar samples are clustered together. For instance, low-load coking data and early-stage high-load data may be incorrectly assigned to the same cluster, resulting in fragmented and non-physical partitions.

To address these issues, a segment-wise method combining change point detection and clustering is proposed.

2.1.1. Data Preprocessing

The historical industrial time series X comprises p variables across T sampling instances.

$$X = \begin{Bmatrix} x_1^1, x_1^2, \ldots, x_1^p \\ x_2^1, x_2^2, \ldots, x_2^p \\ \vdots \\ x_T^1, x_T^2, \ldots, x_T^p \end{Bmatrix} \tag{1}$$

Firstly, missing values are removed and outliers are identified using the Pauta criterion (3σ rule). Subsequently, the Filter-Wrapper feature selection method proposed in our previous work is employed to reduce data dimensionality [43]. To eliminate the influence of different measurement scales, all selected features are normalized using the Z-score method:

$$\tilde{X} = \frac{X - \mu}{\sigma} \tag{2}$$

where, μ and σ denote the mean and standard deviation, respectively.

To address the high-dimensional, noisy, and nonlinear nature of petrochemical time-series data, TS2Vec is first employed to learn compact representations that capture temporal dynamics and inter-variable correlations [44–46], thereby providing a stable embedding space for subsequent structural analysis under process drift and noise. Based on this learned representation space, change point detection is performed to segment the time series into homogeneous intervals, rather than operating on raw measurements.

Specifically, TS2Vec employs a self-supervised contrastive learning framework based on temporal context consistency. Its encoder consists of stacked dilated causal convolutional layers that capture temporal dependencies at multiple scales and generate latent temporal representations. For an input time series $\tilde{X}_t$, the latent representation at time t is defined as follow:

$$z_t = f_\theta(\tilde{X}_t) \tag{3}$$

To improve robustness to industrial noise and local perturbations, temporal cropping and masking are applied to generate multiple augmented views of each time series. Positive pairs are constructed from different views of the same sequence, while views from different temporal contexts are treated as negatives. The model is trained using a hierarchical temporal contrastive loss, which enforces consistency between positive pairs and discriminability from negative samples, enabling multi-scale temporal representation learning. The contrastive loss function is defined as follows:

$$\mathcal{L} = -\frac{1}{T}\sum_{t=1}^{T} log\frac{exp(sim(p_t, p_t^+)/\tau)}{\sum_{j\neq t} exp(sim(p_t, p_j^-)/\tau)} \tag{4}$$

In this formulation, $sim(\cdot,\cdot)$ denotes cosine similarity, and τ is the temperature parameter. p_t^+ denotes the positive sample, while p_j^- denotes the negative sample.

The model is trained using the Adam optimizer with weight decay regularization to improve training stability and reduce the risk of overfitting. After training, the representation $P = \{p_t\}_{t=1}^{T}$ is used as input for change point detection.

2.1.2. Change Point Detection

Change point detection is used to segment time series into homogeneous intervals. It detects points where statistical properties change significantly [42,47,48]. In this study, a change point is defined as a time instant at which the statistical distribution or operational behavior of a time series changes significantly. Such points reflect local variations in process dynamics and do not necessarily correspond to transitions between operating conditions. Because industrial cracking furnaces commonly exhibit gradual process drifts, multi-scale fluctuations, and periodic operational adjustments, the number of detected change points is typically greater than the final number of operating conditions. Consequently, the primary goal of this detection step is to partition long-term time series into segments with relatively homogeneous statistical characteristics, thereby providing temporally consistent data for subsequent operating condition clustering.

To achieve this objective, TS2Vec latent representations are used to characterize process variations. The Euclidean distance $D(t)$ between adjacent temporal embeddings is calculated to quantify dynamic changes between consecutive time steps. A moving-average smoothing strategy is then applied to the distance sequence to suppress measurement noise and high-frequency fluctuations, yielding a more robust change point score.

$$D(t) = \|p_{t+1} - p_t\|_2 \tag{5}$$

$$\widetilde{D}_t = \frac{1}{w}\sum_{i=t-w/2}^{t+w/2} D(i) \tag{6}$$

where w denotes the length of the window.

To reduce false detections caused by noise and local fluctuations, a dual-window comparison strategy is adopted. Unlike the smoothing window used for noise suppression, the comparison windows are selected to be sufficiently larger than the smoothing scale to capture the overall statistical characteristics of neighboring time periods. A potential change point is confirmed when the relative difference φ_t between adjacent windows exceeds a threshold ε. The window size is selected to be sufficiently larger than the smoothing scale to ensure robustness. Statistical validation is further performed using the Kruskal-Wallis test, where ranked samples R_j are used to compute the test statistic U for assessing distributional differences between segments. This procedure effectively reduces false detections caused by local noise, random fluctuations, and transient disturbances.

$$\varphi_t = \frac{|R(t) - L(t)|}{L(t) + \epsilon} \tag{7}$$

$$L(t) = \frac{1}{W}\sum_{i=t-W}^{t-1} \widetilde{D}(i),\ R(t) = \frac{1}{W}\sum_{i=t}^{t+W1} \widetilde{D}(i) \tag{8}$$

$$U = \frac{12}{N(N+1)}\sum_{j=1}^{k}\frac{R_j^2}{n_j} - 3(N+1) \tag{9}$$

The sequence is thus divided into dynamic consistent segments. Each segment is represented by its mean feature vector:

$$c^{(n)} = \frac{1}{L_n}\sum_{t\in n} p(t) \tag{10}$$

Given that physical processes such as coke accumulation, heat transfer degradation, and control adjustments evolve gradually, transitions between operating conditions in cracking furnaces typically occur over several hours rather than instantaneously. Therefore, strict point-to-point matching is impractical, and an event-level verification strategy with a temporal tolerance threshold is adopted. Based on the plant sampling interval, historical operating data, and process dynamics, the threshold is set to 360 sampling points (12 h). This setting accounts for the gradual evolution of operating conditions and the response lag inherent in industrial measurements.

2.1.3. DPC-SNN Clustering

After segmenting the time series into statistically homogeneous intervals, clustering is performed to identify operating conditions with similar characteristics. Traditional clustering methods often encounter difficulties when applied to complex industrial process data. K-means struggles to represent non-convex cluster structures, while Gaussian mixture models (GMM) rely on distributional assumptions that may not hold for strongly nonlinear industrial processes. Hierarchical clustering is computationally expensive, and Density-based spatial clustering of applications with noise (DBSCAN) often degrades in multi-density and high-dimensional spaces.

To address these limitations, Density peak clustering (DPC) is adopted, as it identifies cluster centers based on local density and relative distance without requiring a predefined number of clusters. To further improve robustness under heterogeneous density distributions and noisy conditions, the Shared nearest neighbor (SNN) strategy is introduced to redefine similarity using shared neighbors. By combining global density discrimination with local neighborhood structure, the resulting DPC-SNN framework provides robust operating-condition identification for ethylene cracking furnaces characterized by gradual coking evolution, load fluctuations, slow operating drift, and strong multivariable coupling [49,50].

The local density ρ_i is calculated:

$$\rho_i = \sum_{j=1}^{n} \exp\left(-d_{ij}^2/d_c^2\right) \tag{11}$$

where d_{ij} denotes the SNN distance and d_c is the cutoff parameter. A larger ρ_i indicates a denser region. The minimum distance δ_i to any point with higher density is then obtained. The cluster center criterion is defined as $\gamma_i = \rho_i \cdot \delta_i$, and points are ranked accordingly. The top K points are selected as cluster centers, and the remaining points are assigned accordingly.

In industrial ethylene cracking, operating conditions are typically stable over long periods. To suppress spurious transitions, temporal continuity and duration constraints are introduced. Short segments are merged into adjacent dominant conditions to ensure physical consistency. Cluster-wise mean features are then computed and combined with process knowledge to map results into interpretable operating conditions and stages. Finally, an online random forest classifier trained on offline labels is employed for real-time condition identification. A consistent feature pipeline is maintained, and condition labels with confidence scores are obtained via ensemble voting, improving robustness against transient fluctuations.

2.2. Condition-Dependent Predictive Modeling

The complex dynamics of ethylene cracking processes challenge traditional mechanistic and linear models in achieving both accuracy and robustness within MPC frameworks [51]. To address this issue, a multi-scale Transformer (MS-Trans) predictor is developed as the condition-specific internal model of the MPC framework

to predict future trajectories of key variables. Figure 2 shows the model architecture, including data preprocessing, multiscale feature extraction, Transformer modeling, and output layers. A noise injection strategy is introduced during training to improve robustness.

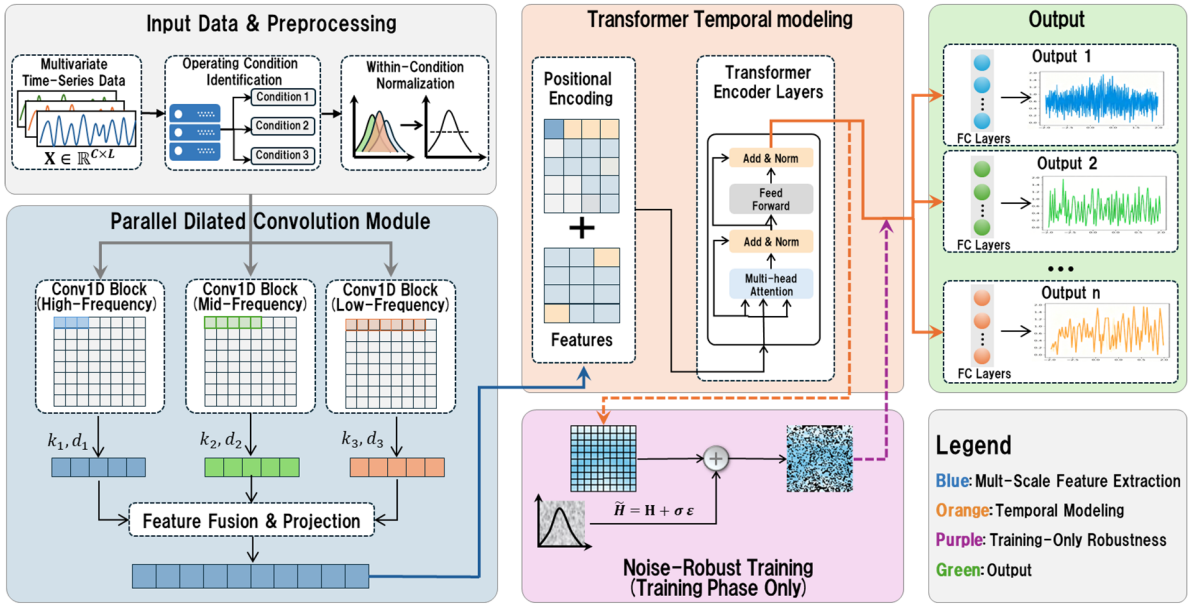

Figure 2. Architecture of the MS-Trans model.

2.2.1. Multiscale Feature Extraction

To capture both high-frequency disturbances and low-frequency trends, a multiscale convolution module is employed. Temporal features are extracted using parallel convolutional branches with different kernel sizes and dilation rates, enabling feature extraction across multiple time scales [52,53].

For the input series X, the multi-scale convolution embedding is defined as:

$$E = \mathrm{Concat}\left(\mathrm{Conv}_{k_1,d_1}(\mathrm{X}), \mathrm{Conv}_{k_2,d_2}(\mathrm{X}), \ldots, \mathrm{Conv}_{k_i,d_i}(\mathrm{X})\right) \tag{122}$$

where k_i and d_i denote the kernel size and dilation rate.

2.2.2. Transformer-based Temporal Modeling

The extracted features are then fed into a Transformer encoder, where the self-attention mechanism captures long-range dependencies among variables, improving the modeling of complex variable interactions [54].

To preserve temporal structure, a learnable positional encoding P is introduced to maintain temporal order within the model.

$$Z = E + P \tag{13}$$

where E denotes the input embedding.

The self-attention mechanism is defined as:

$$Attention(Q, K, V) = softmax\left(QK^T/\sqrt{d_k}\right)V \tag{14}$$

where Q, K, V denote query, key, and value.

A feedforward network extracts nonlinear features. The final representation is obtained with residual connections and normalization:

$$Z' = LayerNorm(MultiHead(Z) + Z) \tag{15}$$

$$H = LayerNorm(FFN(Z') + Z') \tag{16}$$

This representation effectively captures the multiscale dynamic evolution characteristics of the cracking furnace process.

2.2.3. Noise-Robust Training Strategy

Industrial process data are inherently affected by measurement noise and operational disturbances. To improve model robustness, a time-step-scheduled Gaussian perturbation strategy is introduced as a data augmentation mechanism. During training, Gaussian noise is injected into the hidden representation H produced by the Transformer encoder. The total number of time steps is set to $T = 1000$. At each training iteration, a time step t is sampled from a uniform distribution:

$$t \sim Uniform(0, T) \tag{17}$$

A cosine-based scheduling function is then used to determine the signal retention coefficient:

$$\alpha(t) = \cos^2\left(\frac{t}{T} \cdot \frac{\pi}{2}\right) \tag{18}$$

The perturbed representation is constructed as:

$$\widetilde{H} = \sqrt{\alpha(t)}\, H + \sqrt{1 - \alpha(t)}\, \varepsilon, \varepsilon \sim \mathcal{N}(0, I) \tag{19}$$

In this formulation, $\alpha(t)$ controls the signal preservation level, and $1 - \alpha(t)$ determines the noise injection strength. The perturbation magnitude is fully governed by the time-step scheduling function, without introducing additional tunable noise-intensity hyperparameters.

This strategy exposes the model to varying perturbation levels across training iterations, improving robustness and generalization under noisy industrial conditions. Noise injection is applied only during training and disabled during online prediction to ensure deterministic and efficient outputs.

Multiple variables (e.g., coil outlet temperature (COT) and ethylene yield) are predicted using a multitask architecture, as expressed below.

$$\hat{y}_i = f_i(h_T), i = 1, \ldots, M \tag{20}$$

where h_T denotes the hidden state and $f_i(\cdot)$ is the linear projection head. This design enables variables to share underlying dynamics while maintaining independent mappings, accommodating their distinct dynamic behaviors.

2.2.4. Prediction Error Compensation

The model generates short-term predictions from historical data for control optimization and is trained under specific operating conditions to support condition-aware model switching across regimes, thereby improving MPC performance in nonlinear and non-stationary scenarios. To mitigate the continuous accumulation of systematic errors during long-term operation, including coking, heat transfer degradation, and sensor drift, an offset-free mechanism is incorporated into the prediction layer for real-time bias compensation.

$$\tilde{Y}_{t+i} = \hat{Y}_{t+i} + d_t \tag{21}$$

where $d_t = Y_t - \hat{Y}_t$ is the estimated output bias at time t, which is assumed to remain constant over the prediction horizon.

The predicted trajectories are generated as the internal model outputs of the MPC framework, providing the basis for subsequent control optimization.

2.3. Condition-Aware Adaptive MPC Strategy

The complex reactions and coking in ethylene cracking furnaces pose long-term adaptation challenges for traditional MPC. To address this, a CA-AMPC framework is proposed to adaptively adjust prediction models, control weights, and horizon parameters based on operating condition recognition. As shown in Figure 3, the system performs condition identification, state estimation, and parameter updating using real-time data. Optimization is carried out using the sequential least squares programming (SLSQP) algorithm. A multistage heuristic fallback strategy is activated upon convergence failure, followed by a safety check before control execution.

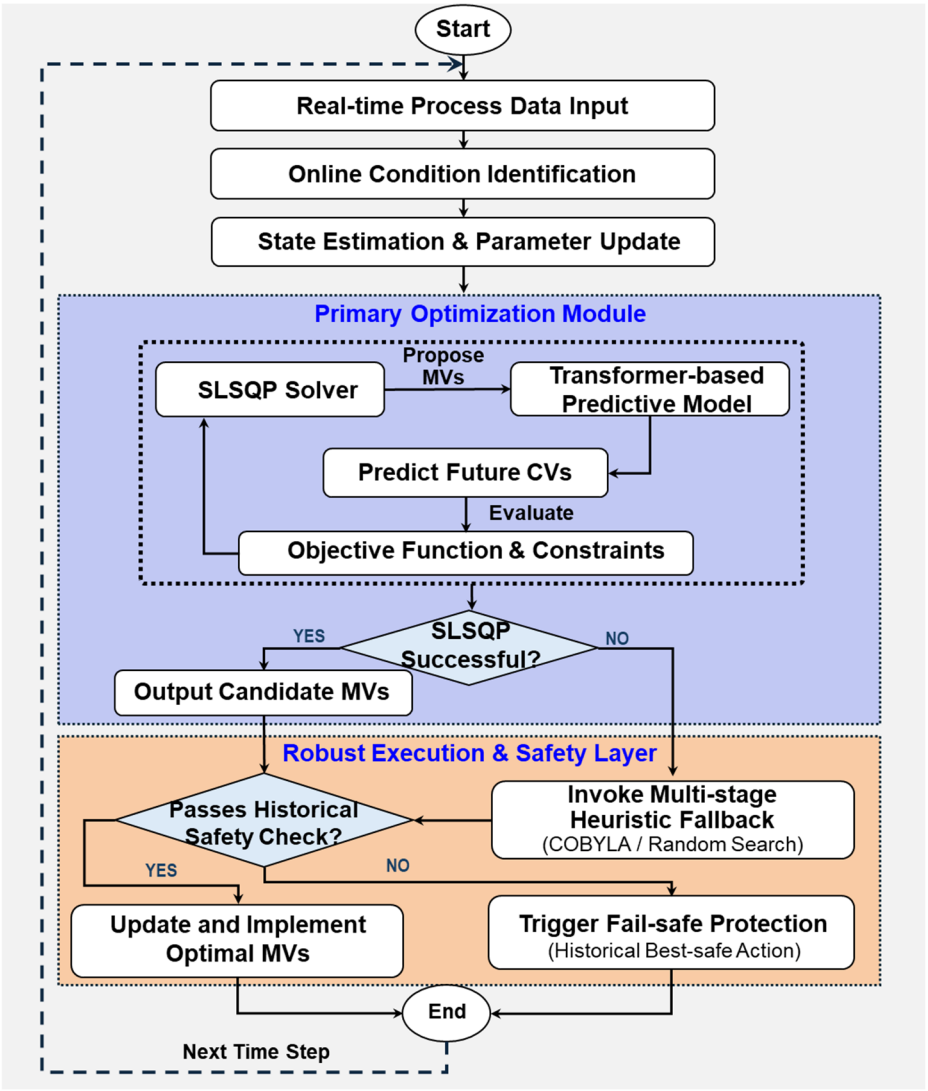

Figure 3. Flowchart of the CA-AMPC execution process.

2.3.1. Control Objective Formulation

In industrial ethylene cracking processes, ethylene yield is highly sensitive to operating variables such as feed flow rate and reaction temperature. Direct yield maximization may lead to significant operational fluctuations, reactor temperature drops, and safety risks. To address this, a multi-objective function is formulated to balance economic, stability, and safety considerations. The optimization problem over the prediction horizon N_p and control horizon N_c is defined as follows:

$$\min_{\Delta u} J = J_{econ} + J_{safe} + J_{smooth} + J_{flux} + J_{surge} \tag{22}$$

The constraints include model state constraints, bounds of the manipulated variables, and move constraints, as follows:

$$s.t.\ \ x(k+1) = f\big(x(k), u(k)\big) \tag{23}$$

$$u_{min} \le u(k+i) \le u_{max} \tag{24}$$

$$\Delta u_{min} \le \Delta u(k+i) \le \Delta u_{max} \tag{25}$$

The components of the objective function define the operational targets of the cracking furnace, as summarized in Table 1.

Table 1. Summary of multi-objective function components.

Formula	Objective
$J_{econ} = -\sum_{i=1}^{N_p} w_{eth}\ \hat{y}_{eth}(k+i\|k)$	Maximization of ethylene yield
$J_{safe} = \sum_{i=1}^{N_p}\sum_{c=1}^{2} w_C \cdot max(0, \hat{T}_C(k+i\|k) - T_{C,ref} - db_C)^2$	Stabilization near setpoint within dead zone
$J_{smooth} = \sum_{i=0}^{N_{c-1}} w_{mv}\left(u_{k,1} - u_{k,prev}\right)^2$	Penalization of single-step setpoint changes
$J_{flux} = -w_{tp}\sum_{i=1}^{N_p}(F_{total}(k+i\|k)\cdot \hat{y}_{eth}(k+i\|k))$	Penalty on unrealistic high-yield low-load operation
$J_{surge} = w_s \sum_{i=0}^{N_c-1} max\left(0, \frac{F_{total}(k+i\|k) - F_{total}(k+i-1\|k)}{F_{total}(k-1)+\in}\right)^2$	Penalty on total feed flow increase

2.3.2. Bayesian Optimization

Traditional MPC relies on fixed control parameters, whereas reaction kinetics and heat transfer vary across operating conditions, often leading to oscillations or degraded performance. To address this, a condition-specific offline optimization and online smooth switching mechanism is proposed.

During the offline stage, Bayesian optimization is performed for each operating condition to determine optimal hyperparameters $\theta = \{w_{eth}, w_C, w_{mv}, N_p, N_c\}$. Here, w_{eth}, w_C, and w_{mv} represent weights for ethylene yield, the controlled variables (CVs) tracking, and the manipulated variables (MVs) penalty, respectively. To reduce the optimization dimensionality and ensure safety, the remaining weights are fixed based on process and equipment constraints.

To handle scale inconsistencies among objectives, continuous weights are sampled from a log-uniform distribution, while N_p and N_c are defined in discrete spaces under the constraint $N_p \geq N_c$. Fitness evaluation is conducted via closed-loop dynamic simulation rather than single-step assessment. Historical states are sampled as initial conditions, and a trajectory of length T_{sim} is simulated for each candidate θ. Infeasible configurations causing solver failure or divergence are heavily penalized to ensure stable optimization. A Gaussian process surrogate models the mapping between θ and average cost $J_{avg}(\theta)$, and expected improvement is used for balancing global exploration and local exploitation.

$$J_{avg}(\theta) = \frac{1}{n}\sum_{j=1}^{n}(\sum_{i=1}^{T_{sim}} J_j(i|\theta) \tag{26}$$

During the online stage, parameters are updated based on condition identification. Since operating conditions evolve gradually rather than abruptly, direct switching of models and parameters may induce control surges, oscillations, or constraint violations. To address this, a smooth switching mechanism is introduced, where model outputs and hyperparameters of adjacent conditions are linearly interpolated over a transition window W_{trans}:

$$\hat{\mathrm{y}}(t) = (1-\alpha(t))\hat{\mathrm{y}}^{(i)}(t) + \alpha(t)\hat{\mathrm{y}}^{(j)}(t), \alpha \in [0,1] \tag{27}$$

$$\hat{\theta}(t) = (1-\alpha(t))\hat{\theta}^{(i)}(t) + \alpha(t)\hat{\theta}^{(j)}(t), \alpha \in [0,1] \tag{28}$$

In this formulation, $\hat{\mathrm{y}}^{(i)}$, $\hat{\theta}^{(i)}$, $\hat{\mathrm{y}}^{(j)}$ and $\hat{\theta}^{(j)}$ denote the prediction outputs and hyperparameter sets before and after transition, respectively. The interpolation factor α increases over time, ensuring smooth evolution of predictions and control weights within the transition window and enabling stable switching between operating conditions.

2.3.3. Hierarchical Optimization and Safety Assurance

To address the computational challenges of highly nonlinear cracking furnaces, a hierarchical optimization and safety mechanism is embedded within each CA-AMPC control cycle. Disturbances are estimated from historical data and compensated using exponential moving average filtering to mitigate coking-induced model deviations and steady-state offsets. The nonlinear optimization problem is solved using SLSQP under incremental constraints and a local feasible region. If SLSQP fails, the solver switches to constrained optimization by linear

approximations (COBYLA), followed by a bounded random search if necessary. A final safety check ensures that all control actions satisfy operational constraints. Unsafe or overly aggressive strategies are replaced with conservative historical trajectories to prevent process hazards and ensure that the Distributed Control System (DCS) always receives feasible control inputs.

The proposed method is validated using industrial data from an ethylene cracking furnace.

3. Results and Discussion

This study focuses on a million-ton ethylene cracking unit in a refinery as the case study. The unit exhibits typical multi-operating-condition behavior in industrial practice, providing a representative scenario for validating the proposed condition identification and condition-driven adaptive control framework. A simplified process flow diagram is shown in Figure 4. The ethylene cracking furnace includes convection and radiation sections. The convection section preheats feedstock and dilution steam using flue gas heat recovery. After reaching cracking temperature, the feed enters the radiation section for thermal cracking. The products are quenched and then sent to downstream separation and fractionation units.

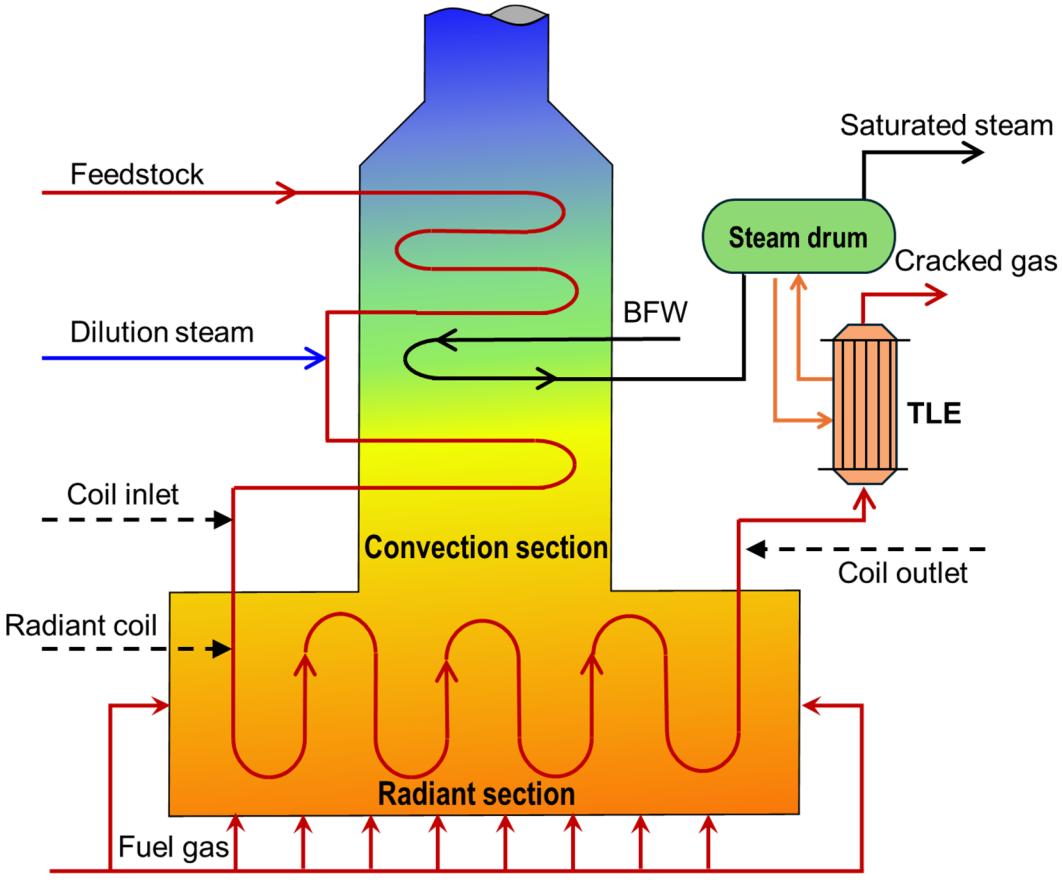

Figure 4. Schematic of the ethylene cracking process.

The data were collected from the DCS over approximately 6 months with a 2-min sampling interval. Missing values and outliers were removed using a Pauta criterion, resulting in 133,077 valid samples. Due to periodic decoking operations, the dataset consists of two discontinuous operating cycles, with 82,679 samples in the first cycle. The preprocessed dataset comprises 214 variables. To mitigate the computational burden and redundancy caused by strongly cross-correlated industrial measurements, a two-stage Filter-Wrapper feature selection strategy is adopted. First, the Filter stage utilizes correlation analysis, mutual information, and distance-based measures to capture linear and nonlinear dependencies, effectively reducing redundant features. Subsequently, the Wrapper stage employs a genetic algorithm combined with support vector regression to iteratively optimize the feature subset based on predictive performance. Through this framework, the initial dataset is reduced to 30 representative variables (Table 2), ensuring stable downstream operating condition identification.

Table 2. Selected process variables after feature selection.

DCS Point Tag	Parameter Name	DCS Point Tag	Parameter Name
TIC001	Quench gas temperature (℃)	PI003	PASS1 radiant section pressure(kPa)
TIC002	COT of furnace A (℃)	PI004	PASS2 radiant section pressure (kPa)
TIC003	COT of furnace B (℃)	PI005	PASS3 radiant section pressure (kPa)
TI001	Radiation section temperature (℃)	PI006	PASS4 radiant section pressure (kPa)
TI002	Preheater A outlet temperature (℃)	PI007	Feed pressure (kPa)
TI003	Preheater B outlet temperature (℃)	FI001	The dilution steam flow (t/h)
TI004	PASS1 outlet temperature (℃)	FI002	Superheated steam flow (t/h)
TI005	PASS2 outlet temperature (℃)	FI003	High-pressure steam flow (t/h)
TI006	PASS3 outlet temperature (℃)	FIC001	Hydrocarbon feed flow (t/h)
TI007	PASS4 outlet temperature (℃)	FIC002	PASS1 naphtha flow (t/h)
TI008	Feed temperature (℃)	FIC003	PASS2 naphtha flow (t/h)
TI009	Furnace A temperature (℃)	FIC004	PASS3 naphtha flow (t/h)
TI010	Furnace B temperature (℃)	FIC005	PASS4 naphtha flow (t/h)
PI001	Cracking gas pressure (kPa)	FIC006	Depropanizer feed flow (t/h)
PI002	Venturi outlet pressure (kPa)	FQIC001	Ethane recycle flow rate (t/h)

3.1. Operating Condition Identification Results

Operating condition identification depends on several key hyperparameters across TS2Vec (e.g., embedding dimension d_{emd}, hidden layer dimension d_{hidden}, number of network layers N_{layer}, learning rate η, and temperature coefficient τ) and the downstream stages (e.g., sliding window size, change point threshold, minimum segment distance, and maximum condition number K). To avoid the computational bottleneck and training instability inherent in a simultaneous global grid search, a two-stage optimization strategy is adopted. First, TS2Vec parameters are optimized to obtain stable and informative latent representations. Based on this fixed representation space, clustering-related parameters are subsequently tuned to maximize the separability and stability of operating-condition identification.

Given the strong nonlinearity and multiscale, gradually evolving nature of ethylene cracking processes, a single metric is insufficient. Therefore, a composite index consisting of the Silhouette (Sil) score, the Davies-Bouldin Index (DBI), and the Calinski-Harabasz Index (CHI) is constructed. The DBI is inversely normalized and fused with Sil and CHI via weighted aggregation, enabling selection of a parameter set that balances statistical separability and physical interpretability. The formulation is given as follows:

$$Score = 0.4 \times Sil_{norm} + 0.3 \times DBI_{norm} + 0.3 \times CHI_{norm} \tag{29}$$

For the TS2Vec module, 64 hyperparameter combinations are evaluated, and the corresponding results are shown in Figure 5. Each curve represents a specific parameter configuration, with the color transitioning from blue to red according to the comprehensive evaluation score from low to high.

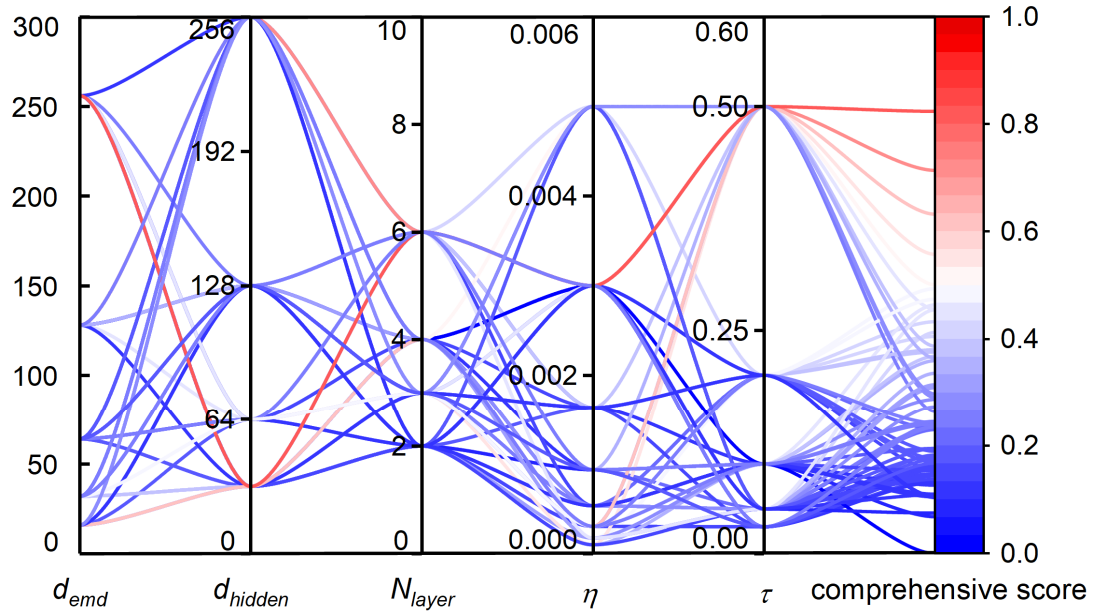

Figure 5. Parallel coordinate plot for TS2Vec hyperparameter evaluation and selection.

The results indicate that different parameter settings have a significant impact on representation quality. The optimal configuration achieves the highest score of 0.83 when $d_{emd} = 256$, $d_{hidden} = 32$, $N_{layer} = 6$, $\eta = 0.003$, and $\tau = 0.5$. This configuration is therefore selected for subsequent operating condition identification.

To verify model convergence, the training and validation loss over 100 epochs are analyzed, as shown in Figure 6. The loss decreases rapidly during the early stage (Epochs 0–20) and stabilizes after approximately 80 epochs. The consistent trends between training and validation curves indicate good convergence and no obvious overfitting.

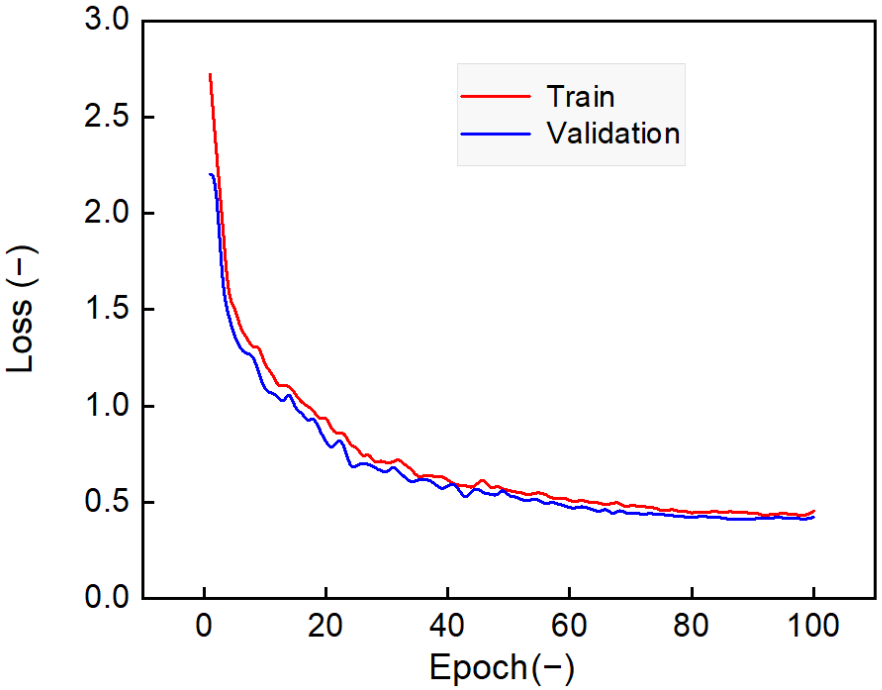

Figure 6. Training and validation loss curves of the TS2Vec model.

To further quantify representation quality, cluster separability is evaluated on raw data, kernel principal component analysis (KPCA) reduced features, and the TS2Vec representation space, as summarized in Table 3. The raw data shows poor separability, with a Sil score of 0.30 and a DBI of 1.24. KPCA improves performance to 0.41 and 0.97, respectively. TS2Vec achieves the best results, with a Sil score of 0.53 and a DBI of 0.74, indicating superior discrimination of operating conditions with nonlinear and temporal dependencies. These results suggest that TS2Vec effectively captures underlying process dynamics through a high-dimensional latent representation. However, because these embedding dimensions are not explicitly designed to correspond to the physical mechanisms of the cracking furnace, the learned representations exhibit limited physical interpretability. Nevertheless, they remain highly suitable for downstream clustering and operating condition identification.

Table 3. Evaluation of cluster separability for different methods.

Method	Sil Score	DBI
TS2Vec	0.53	0.74
KPCA	0.41	0.97
Raw Data	0.30	1.24

Based on the stable and convergent high-quality representation obtained in the previous stage, this section further optimizes the hyperparameters for operating condition clustering. A total of 64 hyperparameter combinations are evaluated, and the corresponding results are visualized using a parallel coordinate plot in Figure 7. The results show that the optimal performance (0.86) is achieved by the red curve, with a sliding window size of 360, a change point detection threshold of 0.025, a minimum segment distance of 360, and a maximum condition number $K = 8$. This configuration is used for subsequent condition identification. In addition, high scoring configurations are mainly distributed in regions with smaller window sizes (360–720), medium penalty thresholds (0.015–0.025), and larger K values. This indicates that the proposed method achieves stable performance within a relatively broad parameter region, rather than relying on a single optimal point, demonstrating certain robustness to parameter variations.

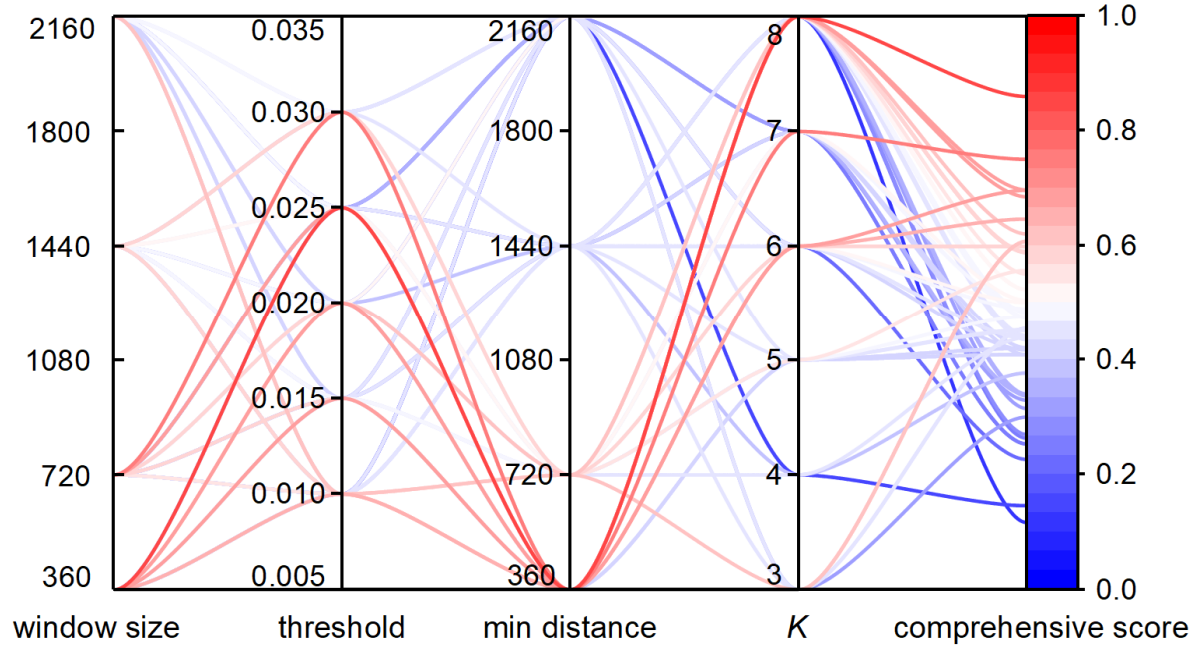

Figure 7. Parallel coordinate plot for hyperparameter evaluation and selection.

Figure 8 illustrates the results of change point detection using ethylene yield as a representative variable. As shown in Figure 8a, the original time series (blue curve) is segmented by 104 detected change points (red dashed lines), corresponding to significant shifts in statistical properties. These points divide the long-term sequence into intervals with relatively consistent dynamics, forming the basis for subsequent regime identification.

To further characterize the identified segments, Figure 8b projects multivariate process variables, including concentration, temperature, and pressure, into a two-dimensional space using principal component analysis (PCA) after standardization. Each bubble represents an operating segment, with coordinates defined by the mean scores of PC1 and PC2. The bubble size is defined as the sum of standard deviations of PC1 and PC2, reflecting intra-segment variability and serving as an indicator of operating stability, while color differentiates individual segments.

The results show a clear clustering structure of operating segments in the reduced space, indicating strong statistical separability induced by change point detection. Most segments exhibit small bubble sizes, corresponding to stable operating states, whereas larger bubbles mainly occur during transition periods. Overall, the proposed segmentation strategy effectively decomposes the non-stationary process into dynamically consistent and physically meaningful operating intervals.

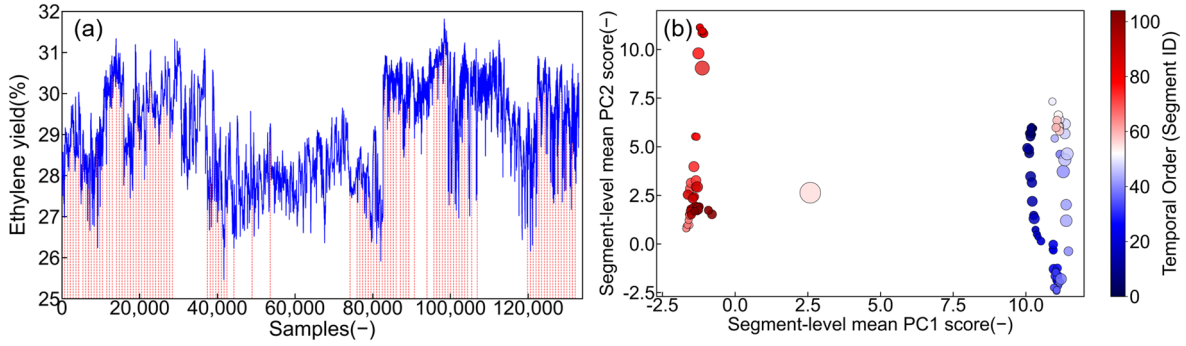

Figure 8. Change point detection based on ethylene yield: (**a**) Detection of inflection points; (**b**) Two-dimensional PCA projection of segmented operating states.

Figure 9 illustrates the operating condition identification results based on DPC-SNN clustering method using ethylene yield as a representative indicator. As shown in Figure 9a, most samples are located in low-density regions of the decision graph, while four cluster centers are automatically identified in high-density regions. Figure 9b shows the temporal evolution of the identified conditions, where four operating regimes are observed with a non-cyclic and unidirectional transition pattern, consistent with the irreversible nature of coking accumulation and

operational adjustments. Cluster 3 exhibits a short duration of 8 days and is identified as a transitional state. To avoid over-segmentation, an adaptive merging strategy based on geometric distance is applied. The centroid of short-duration segments is computed in the feature space, and distances to adjacent clusters are evaluated. As shown in Figure 9c), Cluster 3 is closer to Cluster 4 (distance 3.9), and is therefore merged into Cluster 4, ensuring physical consistency and temporal continuity. Figure 9d maps the final clustering results back to the ethylene yield time series. Clear differences in mean levels and fluctuation ranges are observed across operating conditions. Specifically, Clusters 1 and 3 exhibit higher variability and relatively higher yield, whereas Cluster 2 shows lower yield levels.

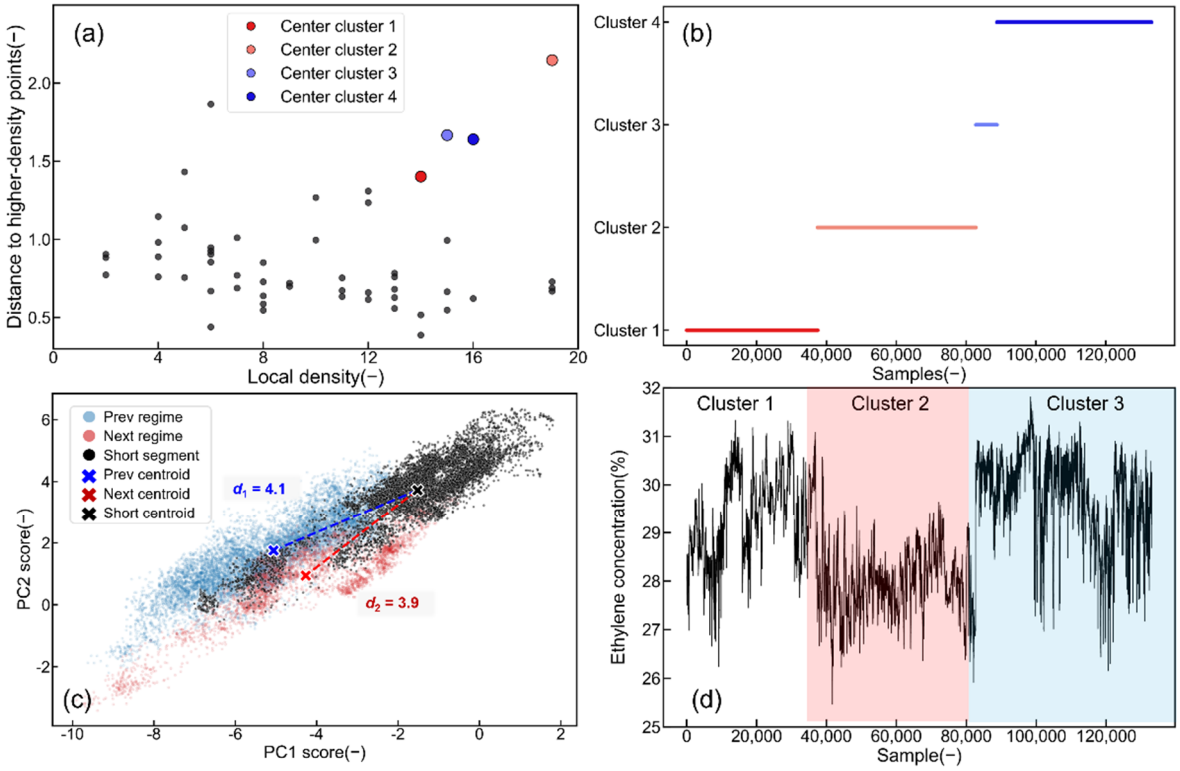

Figure 9. Operating condition identification results: (**a**) DPC-SNN decision graph; (**b**) Temporal distribution of clusters; (**c**) Centroid distance for segment merging; (**d**) Final identified conditions based on ethylene yield.

The identified condition transition point (82,439) closely matches the actual decoking record (82,679), with a relative error of only 0.29%, providing strong evidence of the accuracy of the proposed condition identification method. Representative operating characteristics of each condition are summarized in Table 4.

Table 4. Key process parameters across the identified operating conditions.

DCS Point Tag	Parameter Name	Condition 1	Condition 2	Condition 3
FIC001	Hydrocarbon flow rate(t/h)	49.04	49.03	53.60
TIC001	Quenched gas temperature(°C)	216.69	215.92	223.06
TI001	Radiant section temperature(°C)	973.73	991.86	980.10
FQIC001	Ethane recycle flow rate (t/h)	27.09	26.93	26.17
PI001	Cracking gas pressure(kPa)	127.12	121.19	72.57
TIC002	COT of furnace A (°C)	850.99	854.37	866.01
FI001	Dilution steam flow rate (t/h)	18.37	17.92	14.36
PI002	Venturi outlet pressure(kPa)	156.75	181.71	212.01
AI001	Ethylene yield (%)	29.38	27.96	29.81

As shown in Table 4, Condition 1 corresponds to normal-load early-coking condition, where minimal coking has negligible impact on flow resistance and heat transfer, resulting in an ethylene yield of 29.38%. With continued operation, coke deposition intensifies, and the unit transitions to Condition 2, representing a normal-load severe-coking condition. Although the feed rate remains relatively constant, the Venturi outlet pressure increases significantly, indicating higher flow resistance. Meanwhile, the COT rises from 850.99 °C to 854.37 °C to compensate for reduced heat transfer efficiency, leading to decreased selectivity and a reduced yield of 27.96%.

After decoking, the unit enters Condition 3, characterized by post-decoking high-load condition, high cracking temperature, and low cracked gas pressure. The elevated temperature enhances primary cracking reactions, while the reduced hydrocarbon partial pressure suppresses coke formation [55]. In addition, the higher feed load shortens residence time, limiting secondary reactions and increasing the ethylene yield to 29.81%. Overall, these results demonstrate clear differences in reaction selectivity, heat transfer, and flow resistance across operating conditions, confirming that the proposed framework successfully identifies physically meaningful and control-relevant process states.

3.2. Prediction Model Performance for Control

Considering the redundancy in high-frequency DCS time-series data, direct training on the full dataset increases computational cost and may introduce overfitting to local noise. To address this, a uniform downsampling strategy is applied for each operating condition, resulting in 5000 representative samples while preserving the global dynamics and evolutionary trends of the process. To avoid data leakage and maintain temporal causality, a strict time-series split is adopted with a 9:1 ratio. The first 90% of each condition is used for training and parameter optimization, while the remaining 10% is reserved for independent testing to evaluate generalization performance.

Figure 10 presents the prediction results of the MS-Trans model for key variables, including ethylene yield and the COT on both sides, denoted as COT(A) and COT(B), under three typical operating conditions. Each condition is modeled independently, and the corresponding sub-model is invoked during testing based on the identified condition label. The results show that the model accurately tracks variations in both temperature and yield across different conditions, providing reliable multi-step predictions for subsequent control optimization.

For COT, the mean absolute percentage error (MAPE) remains within 0.3%. A slightly higher error is observed in Condition 2 due to intensified coking, which increases thermal resistance and introduces additional disturbances, thereby weakening the input-output mapping. For ethylene yield, the MAPE ranges from 1.54% to 1.66% across all conditions, indicating stable prediction performance. This is because coking primarily affects local heat transfer, whereas yield reflects the overall reaction outcome and is therefore less sensitive to localized disturbances.

To systematically evaluate different modeling strategies for predicting key variables of the cracking furnace, four model configurations are compared: (i) MS-Trans without operating condition distinction (Baseline 1), (ii) Transformer with condition distinction (Baseline 2), (iii) Diffusion model with condition distinction (Baseline 3), and (iv) the proposed MS-Trans with condition distinction. The comparative results are shown in Figure 11. The proposed model achieves the best performance across all metrics. For ethylene yield prediction, it attains a root mean square error (RMSE) of 0.61, representing a reduction of over 50% compared to Baseline 1, and further improvements of approximately 12% and 15% over Baselines 2 and 3, respectively. For COT prediction, the RMSE for COT(A) is reduced to 2.80, corresponding to a 60% improvement over Baseline 1, with similar trends observed for COT(B).

These results demonstrate that incorporating operating condition distinction significantly enhances prediction accuracy and stability in non-stationary processes, which is critical for maintaining reliable model performance within the MPC framework.

The performance gains stem from the complementary effects of multiple modeling mechanisms. Multi-scale convolution embedding captures both high-frequency disturbances and low-frequency evolution patterns, while the Transformer attention mechanism improves long-range dependency modeling. In addition, hidden-state noise injection enhances robustness under industrial disturbances. Combined with condition-specific modeling, this design enables the model to adapt to distinct dynamic regimes and avoids the degradation associated with unified modeling of non-stationary data, thereby supporting stable and accurate predictive control.

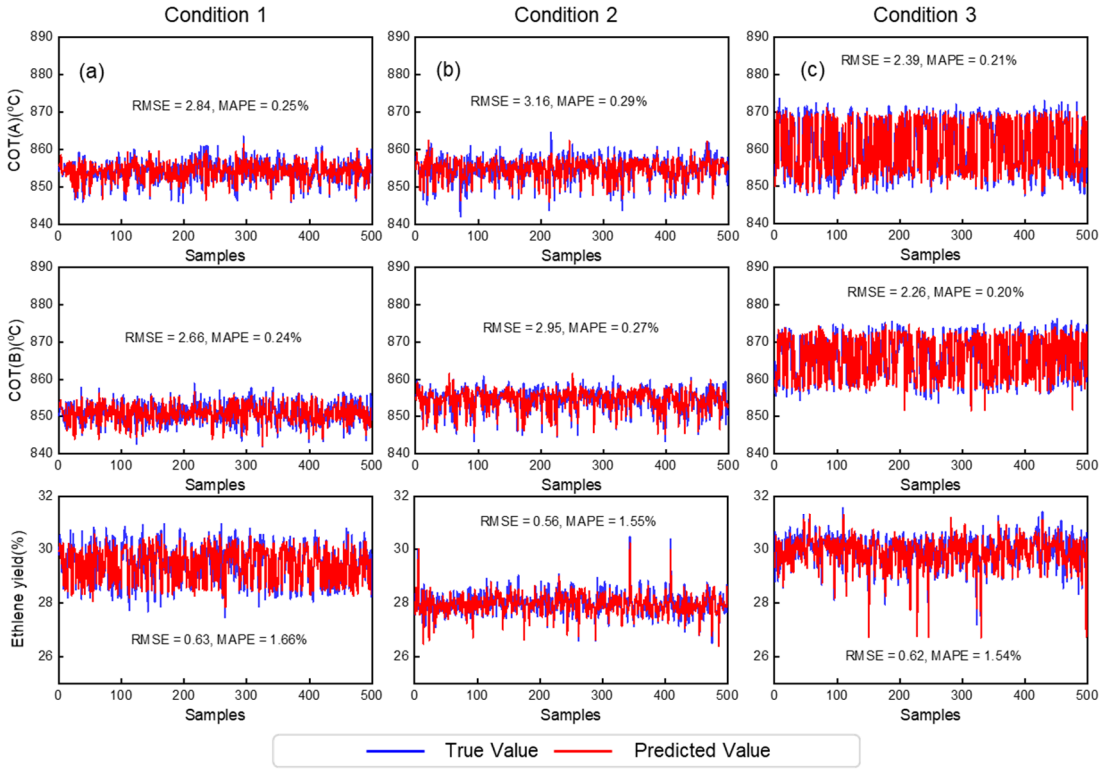

Figure 10. Prediction results of COT and yield: (**a**) Condition 1; (**b**) Condition 2; (**c**) Condition 3.

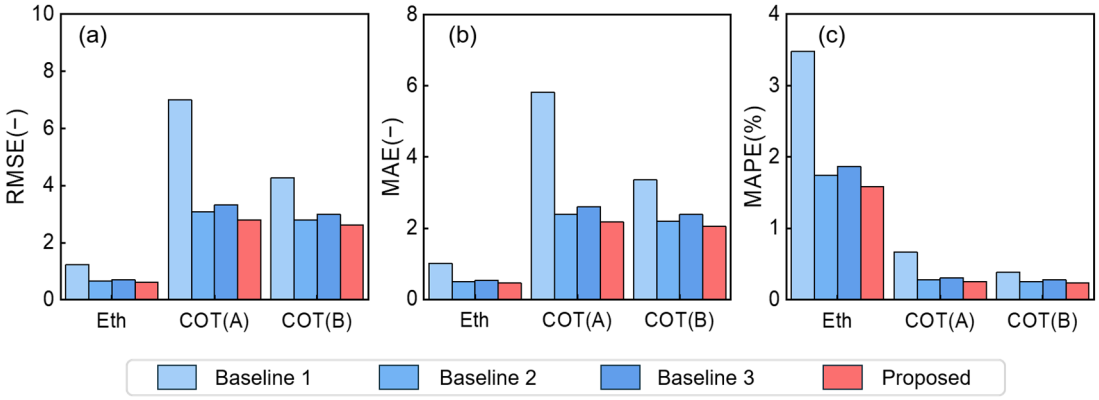

Figure 11. Comparison of predictive model performance across different methods: (**a**) RMSE; (**b**) MAE; (**c**) MAPE.

3.3. Control Performance Evaluation

This paper evaluates the proposed CA-AMPC framework using operational data from an industrial ethylene cracking furnace, comparing its performance against the plant's original PID control system and a fixed-parameter MPC baseline. To ensure a fair comparison, both MPC methods share identical configurations, including datasets, variables, objectives, constraints, optimization solvers, and prediction/control horizons. Furthermore, their hyperparameters are tuned using the same Bayesian optimization strategy. The fixed-parameter MPC is trained once on the full dataset and remains static. Consequently, the only structural difference between the two MPC schemes is the proposed operating condition identification and adaptive mechanism, ensuring that performance improvements are primarily attributable to this condition-adaptive strategy.

The COT and ethylene yield are selected as CVs. COT reflects reaction severity and governs cracking intensity, while ethylene yield serves as a key economic indicator to maintain operation in a high-selectivity region. Eight MVs are considered based on practical availability. MV1-MV4 denote naphtha feed flow rates for individual furnace passes, MV5-MV6 correspond to light hydrocarbon and recycled ethane feed rates, and MV7-MV8 represent quench oil temperature and high-pressure steam temperature, respectively.

For the operating conditions identified in Section 3.1, Bayesian optimization is employed to determine condition-specific control weights, as shown in Figure 12. Under Condition 1, higher weights are assigned to CVs

to maintain process stability. Under Condition 2, the weights of MVs are increased and greater emphasis is placed on yield to suppress fluctuations and avoid excessive cracking. After decoking, under Condition 3, the constraints are relaxed to enhance control flexibility. These results indicate that the optimized control parameters are consistent with the underlying process characteristics, enabling a balanced trade-off among stability, selectivity, and flexibility. The obtained condition-specific parameters are then integrated into the CA-AMPC framework for dynamic control under varying operating conditions. Figures 13–15 illustrate the dynamic regulation performance of the proposed method under different operating conditions, in comparison with PID control and conventional MPC with fixed parameters.

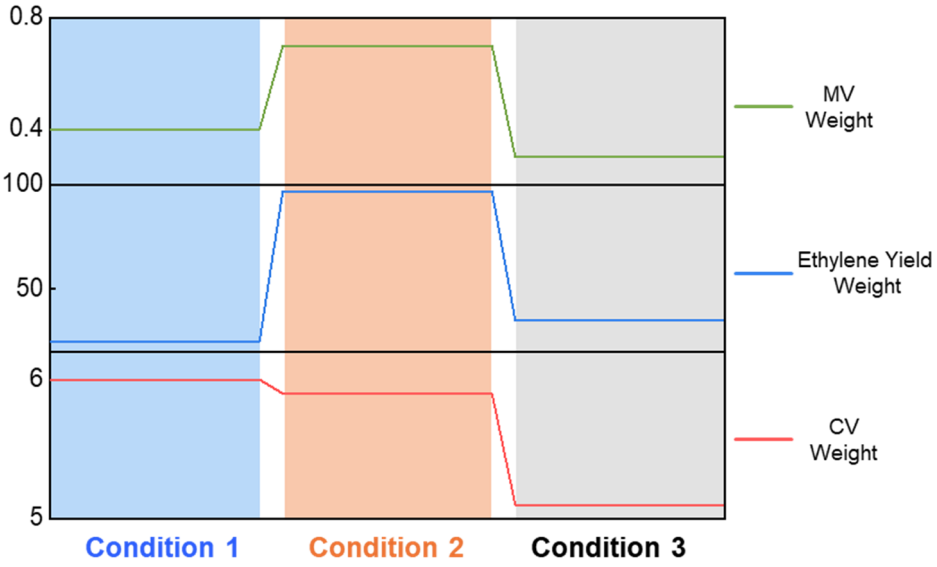

Figure 12. Optimal control weights via Bayesian optimization across operating conditions.

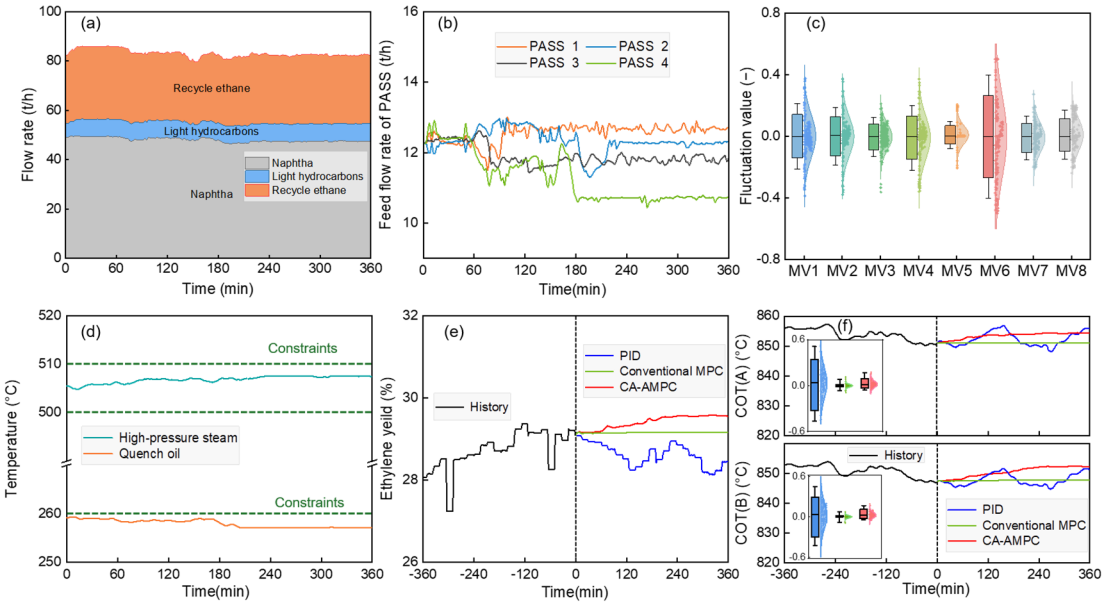

Figure 13. Control performance under Condition 1: (**a**) Feed flow; (**b**) Four-pass naphtha feed flow; (**c**) MVs fluctuation distribution; (**d**) Temperature profiles; (**e**) Ethylene yield comparison; (**f**) COT comparison.

Figure 13 presents the control performance under Condition 1. As shown in Figure 13a, the total feed load remains stable, while individual components exhibit differentiated adjustments. In particular, MV6 shows the largest variation, indicating that the controller preferentially utilizes fast-response variables for disturbance compensation. Figure 13b further reveals staged load redistribution across furnace passes. The system remains stable during 0–60 min, followed by a reduction in the fourth-pass feed between 60–200 min without immediate compensation from other passes, reflecting asynchronous adjustment. After 200 min, the flows stabilize, indicating

the establishment of a new operating equilibrium. This staged redistribution compensates for imbalances in heat transfer and flow among passes. The distribution of manipulated variables in Figure 13c confirms this behavior, where MV6 exhibits the widest range, while other variables remain concentrated. Variables with fast response are actively adjusted, whereas those with larger thermal inertia remain relatively stable. As shown in Figure 13d, key thermal variables, including high-pressure steam and quench oil temperatures, are maintained within safe limits, with the steam temperature operating near its upper bound, indicating effective utilization of the allowable operating space. Figure 13e,f compare control performance. The PID controller exhibits significant oscillations and reduced yield (28–29%), while the fixed-parameter MPC shows conservative behavior with limited improvement (approximately 29.2%). This conservatism arises from globally optimized parameters that over-penalize control actions under this condition, resulting in limited utilization of available operating margins. In contrast, CA-AMPC achieves stable yield enhancement (29.5–30.0%) with reduced COT fluctuations (851–853 °C), demonstrating the effectiveness of condition-specific control adaptation.

Figure 14 illustrates the multivariable cooperative control behavior under Condition 2. As coke deposition increases, heat transfer resistance rises and overall efficiency decreases, leading to higher-frequency feed adjustments compared with the early stage. As shown in Figure 14b, asynchronous redistribution of feed across furnace passes occurs during 0–180 min, reflecting spatial reallocation under uneven coking. The controller reduces feed in degraded passes while increasing it in better-performing ones to mitigate local overheating. This behavior is consistent with Figure 14c, where MV1-MV4 exhibit enlarged adjustment ranges, while MV6 exhibits a relatively small fluctuation range (approximately 0.6), reducing disturbance propagation from fast to slow variables. Figure 14d demonstrates effective constraint handling. Despite large feed-side fluctuations, quench oil and steam temperatures remain within safety limits, due to the constraint-aware optimization mechanism, ensuring safe operation while preserving economic performance. Figure 14e,f show that PID leads to low yield (approximately 28%) due to conservative cooling, while MPC saturates at approximately 29.2% under parameter mismatch. In contrast, CA-AMPC maintains approximately 29.5% yield with controlled COT fluctuations under boundary-active operation, further confirming the advantage of condition-driven parameter adaptation.

Figure 15 illustrates the control behavior under Condition 3. The removal of coke significantly improves heat transfer capacity and reduces process nonlinearity, resulting in enhanced system controllability. As shown in Figure 15a,b, the total feed is rapidly increased from 85 t/h to 95 t/h within 0–60 min and stabilizes near the historical high-load steady-state level, reflecting the natural establishment of the high-load regime rather than any control failure or disturbance-driven abnormal response. During this stage, feed trajectories across the four passes become highly synchronized due to reduced thermal heterogeneity, indicating improved spatial uniformity of the furnace. Figure 15c shows that throughput enhancement is achieved with minor and coordinated MV adjustments. Meanwhile, Figure 15d confirms that key thermal constraints are strictly maintained. The high-pressure steam temperature increases slightly from 503 °C to 505 °C, while quench oil temperature remains stable, indicating effective thermal management under increased load. Figure 15e,f compare control performance. PID exhibits low-frequency oscillations and yield fluctuations (30.230.6%) with a declining trend. Fixed-parameter MPC shows transient oscillations and difficulty maintaining steady operation under high-gain conditions. In contrast, CA-AMPC achieves stable yield improvement to approximately 30.9% through coordinated condition recognition and adaptive control adjustment.

Across the three operating conditions, CA-AMPC exhibits a consistent condition-driven control mechanism that adapts to the changing physical characteristics of the ethylene cracking furnace. Under early coking conditions, the controller compensates disturbances via selective adjustment of fast-response variables and staged load redistribution. As coking intensifies, control emphasis shifts toward high-frequency feed regulation and spatial load reallocation to handle deteriorated heat transfer. After decoking, improved thermal conditions enable synchronized multi-pass feed increases and feedforward compensation, supporting rapid throughput enhancement. Despite these differences, CA-AMPC consistently maintains safety constraints while improving economic performance through condition-dependent adaptation and coordinated multi-timescale control, and constraint-aware optimization.

Overall, the CA-AMPC framework achieves stable operation and yield improvement under varying operating conditions while satisfying safety constraints. Traditional PID and fixed-parameter MPC remain widely used in industry due to their simplicity and robustness, and perform well under relatively stable operating conditions. However, in ethylene cracking furnaces characterized by coke formation, operating condition drift, and strong multivariable coupling, these fixed strategies may gradually suffer from model mismatch. In contrast, CA-AMPC improves adaptability through operating-condition identification and adaptive model selection.

To evaluate its engineering feasibility, the online computational overhead is analyzed. The condition identification module requires 1.71 s on average, while the single-step optimization times are 59.56 s, 50.32 s, and

46.20 s under different operating conditions. The total execution time remains well below the 120 s DCS sampling interval, indicating real-time applicability. From a deployment perspective, CA-AMPC acts as a supervisory optimization layer that can be integrated into existing DCS architectures without modifying the underlying control loops, providing a practical solution for industrial control system enhancement.

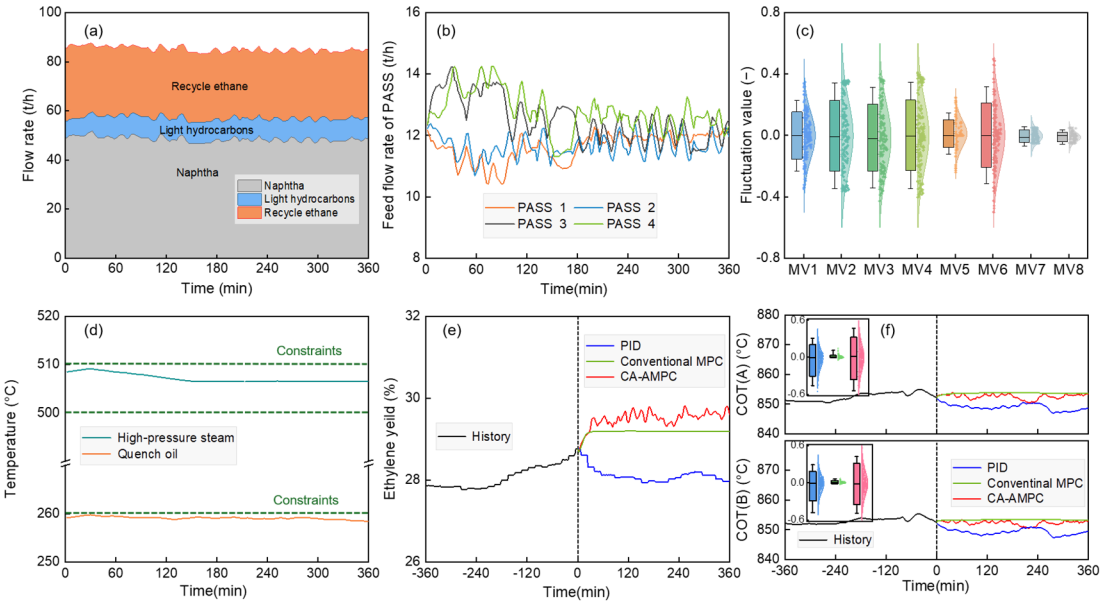

Figure 14. Control performance under Condition 2: (**a**) Feed flow; (**b**) Four-pass naphtha feed flow; (**c**) MVs fluctuation distribution; (**d**) Temperature profiles; (**e**) Ethylene yield comparison; (**f**) COT comparison.

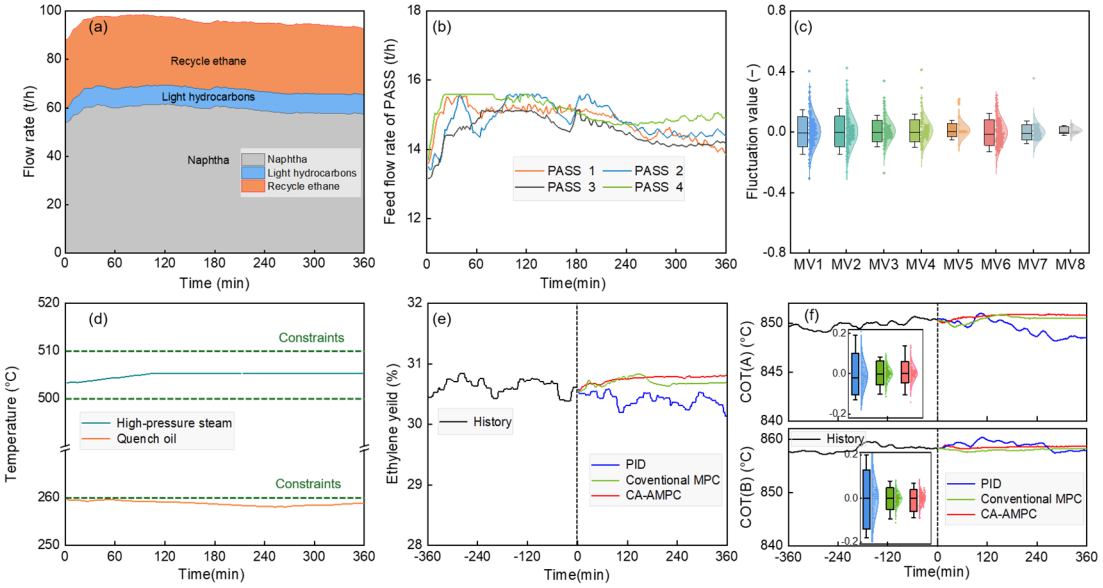

Figure 15. Control performance under Condition 3: (**a**) Feed flow; (**b**) Four-pass naphtha feed flow; (**c**) MVs fluctuation distribution; (**d**) Temperature profiles; (**e**) Ethylene yield comparison; (**f**) COT comparison.

4. Conclusions

In this paper, a CA-AMPC framework is proposed to address challenges arising from strong nonlinearity, multivariable coupling, and operating-condition shifts during long-term operation of an ethylene cracking furnace. The framework introduces an unsupervised condition identification method, which transforms identified conditions into a dynamic decision-making basis for the control layer. Through dynamic model switching, the control strategy is automatically adapted to different operating conditions, enabling process-level dynamic optimization.

Validation on industrial ethylene cracking data demonstrates that the proposed method achieves robust performance across diverse operating regimes. Under normal-load early-coking condition, the controller effectively rejects disturbances through multivariable coordination, maintains furnace tube load balance, and ensures steady operation. Under normal-load severe-coking condition, the strategy performs optimized regulation within constrained operating ranges to mitigate yield degradation while satisfying safety constraints. Under post-decoking high-load condition, the control strategy shifts toward economic optimization, fully exploiting furnace capacity to improve ethylene yield and reduce fluctuations. Under different operating conditions, the yield improvements are approximately 1.0%, 1.5%, and 0.3%, respectively.

Overall, CA-AMPC enables real-time identification of operating-condition transitions and adaptive adjustment of control policies. While strictly satisfying process safety constraints, it achieves coordinated optimization of economic performance. This provides an effective solution for intelligent adaptive control of complex industrial processes.

While the proposed framework demonstrates satisfactory performance under various operating conditions, several limitations remain. First, the current approach is primarily data-driven, and the relationship between latent representations and specific process variables is not yet explicitly established, which limits physical interpretability and generalization to unseen conditions. Second, while segmented modelling alleviates model mismatch to some extent, its extrapolation capability under evolving process dynamics remains limited. Finally, the proposed method currently relies on offline training and has not yet been deployed in an online industrial environment. Future work will focus on integrating first-principles knowledge with data-driven models, developing incremental and online learning mechanisms, and conducting closed-loop industrial deployment to further evaluate long-term robustness, system integration performance, and practical applicability.

Author Contributions

M.L.: conceptualization, methodology, software, writing—original draft preparation, writing—reviewing and editing; M.Z.: investigation, writing—original draft preparation, writing—reviewing and editing; Y.Z.: supervision, visualization, investigation; X.S.: supervision, conceptualization, investigation; X.L.: supervision, writing—reviewing and editing, project administration, funding acquisition. All authors have read and agreed to the published version of the manuscript.

Funding

This work was supported by the National Key Research and Development Program of China (2024YFE0212400).

Institutional Review Board Statement

Not applicable.

Informed Consent Statement

Not applicable.

Data Availability Statement

The raw data used in this study are proprietary and cannot be publicly disclosed due to a non-disclosure agreement with the industrial partner. Processed and anonymized data are available from the corresponding author upon reasonable request.

Conflicts of Interest

The authors declare no conflict of interest.

Use of AI and AI-Assisted Technologies

No AI tools were utilized for this paper.

References

1. Fakhroleslam, M.; Sadrameli, S.M. Thermal/catalytic cracking of hydrocarbons for the production of olefins; a state-of-the-art review III: Process modeling and simulation. *Fuel* **2019**, *252*, 553–566.
2. Sadrameli, S.M. Thermal/catalytic cracking of hydrocarbons for the production of olefins: A state-of-the-art review I: Thermal cracking review. *Fuel* **2015**, *140*, 102–115.

3. Yuan, B.F.; Zhang, Y.; Du, W.L.; et al. Assessment of energy saving potential of an industrial ethylene cracking furnace using advanced exergy analysis. *Appl. Energy* **2019**, *254*, 113583.
4. Hu, G.H.; Zhang, Y.; Du, W.L.; et al. Zone method based coupled simulation of industrial steam cracking furnaces. *Energy* **2019**, *172*, 1098–1116.
5. Shen, W.H.; Tian, Z.; Zhao, L.; et al. Life Cycle Assessment and Multiobjective Optimization for Steam Cracking Process in Ethylene Plant. *ACS Omega* **2022**, *7*, 15507–15517.
6. Shi, H.Y.; Wang, W.Z.; Peng, B.; et al. Multi-step compensated robust predictive cascade control for ethylene cracking furnaces with time delay. *Chem. Eng. Sci.* **2026**, *320*, 122412.
7. Zheng, S.; Zhang, X.Y.; Qi, C.B.; et al. Modeling of heat transfer and pyrolysis reactions in ethylene cracking furnace based on 3-D combustion monitoring. *Int. J. Therm. Sci.* **2015**, *94*, 28–36.
8. Dormido, S. Advanced PID control. *IEEE Control Syst. Mag.* **2006**, *26*, 98–101.
9. Martineau, S.; Burnham, K.J.; Minihan, J.A.; et al. Application of a Bilinear Pid Compensator to an Industrial Furnace. *IFAC Proc. Vols.* **2002**, *35*, 25–30.
10. Ben-Mansour, R.; Badr, H.M.; Araoye, A.A.; et al. Computational analysis of water-submerged jet erosion. *Energies* **2021**, *14*, 3074.
11. Meri, Y.; Siddiqui, O.; Toor, I.U.H.; et al. A detailed review of numerical modeling of flow accelerated corrosion: Challenges and opportunities for the future. *Mater. Corros.* **2024**, *76*, 368–385.
12. Zhang, C.H.; Wang, Z.L. A data-driven strategy for industrial cracking furnace system scheduling under uncertainty. *Chem. Eng. Sci.* **2023**, *277*, 118865.
13. Zhang, R.D.; Xue, A.K.; Wang, S.Q. Dynamic Modeling and nonlinear predictive control based on partitioned model and nonlinear optimization. *Ind. Eng. Chem. Res.* **2011**, *50*, 8110–8121.
14. Zhang, R.D.; Wang, S.Q. Support vector machine based predictive functional control design for output temperature of coking furnace. *J. Process Control* **2008**, *18*, 439–448.
15. Qin, S.J.; Badgwell, T.A. A survey of industrial model predictive control technology. *Control Eng. Pract.* **2003**, *11*, 733–764.
16. Khimani, D.; Mate, S.; Bhartiya, S. Model Predictive Control: Trade-offs between performance and computation time. *IFAC-Pap.* **2024**, *57*, 77–82.
17. Chen, P.; Xu, B.C.; He, W.; et al. Transformer-based model predictive control with feedforward prediction for ammonia injection optimization in SCR denitrification systems. *Process Saf. Environ.* **2025**, *202*, 107804.
18. Jin, Y.K.; Li, J.L.; Du, W.L.; et al. Integrated operation and cyclic scheduling optimization for an ethylene cracking furnaces system. *Ind. Eng. Chem. Res.* **2015**, *54*, 3844–3854.
19. Zhang, Y.; Sha, P.; Wang, M.H.; et al. Toward intelligent and green ethylene manufacturing: An AI-based multi-objective dynamic optimization framework for the steam thermal cracking process. *Engineering* **2025**, *52*, 160–171.
20. Zhao, S.J.; Zhang, J.; Xu, Y.M. Performance monitoring of processes with multiple operating modes through multiple PLS models. *J. Process Control* **2006**, *16*, 763–772.
21. Pipino, H.A.; Adam, E.J. Adaptive model-based predictive control with changing operation points. *Comput. Chem. Eng.* **2025**, *200*, 109188.
22. Hou, Z.S.; Wang, Z. From model-based control to data-driven control: Survey, classification and perspective. *Inf. Sci.* **2013**, *235*, 3–35.
23. Bakhtyari, A.; Seo, J.G. AI-assisted modeling and optimization of large-scale ethylene production by catalytic oxidative dehydrogenation of ethane in a shell-and-tube multi-tubular reactor. *Chem. Eng. J.* **2026**, *529*, 172969.
24. Berreni, M.; Wang, M.H. Modelling and dynamic optimization of thermal cracking of propane for ethylene manufacturing. *Comput. Chem. Eng.* **2011**, *35*, 2876–2885.
25. Nian, X.Y.; Wang, Z.L.; Qian, F. Strategy of changing cracking furnace feedstock based on improved group search optimization. *Chin. J. Chem. Eng.* **2015**, *23*, 181–191.
26. Geng, Z.Q.; Kong, W.K.; Wang, X.T.; et al. Adaptive search based Grey Wolf optimization algorithm for multi-objective optimization of ethylene cracking furnace. *Swarm Evol. Comput.* **2025**, *92*, 101810.
27. Allah, M. AA.; Toor, I.U.H.; Shams, A.; et al. Application of machine learning and deep learning techniques for corrosion and cracks detection in nuclear power plants: A review. *Arab. J. Sci. Eng.* **2024**, *50*, 3017–3045.
28. Li, Q.; Zhang, M.X.; Shi, X.G.; et al. An intelligent hybrid feature subset selection and production pattern recognition method for modeling ethylene plant. *J. Anal Appl. Pyrol.* **2021**, *160*, 105352.
29. Camperos, J.A.; Diaz, C.M.; Cely, M.M.; et al. Dense-gas/liquid two-phase flow pattern recognition using convolutional neural networks and transfer learning. *Int. J. Multiph. Flow* **2026**, *194*, 105479.
30. Wang, C.Y.; Du, M.J.; Jiang, X.; et al. Fuzzy cluster-aware contrastive clustering for time series. *Pattern Recognit.* **2026**, *173*, 112899.
31. Lin, X.W.; Zhao, L.; Shang, C.; et al. Data-driven robust optimization for cyclic scheduling of ethylene cracking furnace system under uncertainty based on kernel learning. *Chem. Eng. Sci.* **2022**, *260*, 117919.

32. Li, H.R.; Wei, Y.X.; Qiu, T. Dynamic Scheduling of ethylene cracking furnaces system leveraging deep reinforcement learning. In *Computer Aided Chemical Engineering*; Manenti, F., Reklaitis, G.V., Eds.; Elsevier: Amsterdam, The Netherlands, 2024; Volume 53, pp. 2989–2994.
33. Cong, D.; Shi, C.J.; Cui, Y.F.; et al. Novel competing evolutionary membrane algorithm based on multiple reference points for multi-objective optimization of ethylene cracking processes. *Chemom. Intell. Lab. Syst.* **2021**, *217*, 104389.
34. Yu, K.J.; While, L.; Reynolds, M.; et al. Cyclic scheduling for an ethylene cracking furnace system using diversity learning teaching-learning-based optimization. *Comput. Chem. Eng.* **2017**, *99*, 314–324.
35. Chiu, J.E.; Fu, S.Z. On-line recognition of mixture control chart patterns using hybrid CNN and LSTM for auto-correlated processes. *Comput. Ind. Eng.* **2024**, *198*, 110674.
36. Zhang, L.X.; Xiang, W.M. Mode-identifying time estimation and switching-delay tolerant control for switched systems: An elementary time unit approach. *Automatica* **2016**, *64*, 174–181.
37. Zhao, S.J.; Zhang, J.; Xu, Y.M. Monitoring of processes with multiple operating modes through multiple principle component analysis models. *Ind. Eng. Chem. Res.* **2004**, *43*, 7025–7035.
38. Zheng, C.; Zhang, Y.; Sha, P.; et al. Optimal scheduling of low-carbon ethylene production system based on deep reinforcement learning: Considering flexible operation under furnace coking and renewable energy fluctuations. *Energy* **2026**, *342*, 139780.
39. Deng, Z.Y.; Han, T.; Cheng, Z.H.; et al. Fault detection of petrochemical process based on space-time compressed matrix and Naive Bayes. *Process Saf. Environ.* **2022**, *160*, 327–340.
40. Han, X.Y.; Tian, S.W.; Romagnoli, J.A.; et al. The real-time multiple operational condition monitoring of ethylene cracking furnace based on the principal component analysis. *Chem. Eng. Trans.* **2017**, *61*, 517–522.
41. Maestri, M.; Farall, A.; Groisman, P.; et al. A robust clustering method for detection of abnormal situations in a process with multiple steady-state operation modes. *Comput. Chem. Eng.* **2010**, *34*, 223–231.
42. Bao, X.Y.; Chen, L.; Zhong, J.S.; et al. A self-supervised contrastive change point detection method for industrial time series. *Eng. Appl. Artif. Intell.* **2024**, *133*, 108217.
43. Zhang, M.X.; Cao, D.F.; Lan, X.Y.; et al. An Ensemble-learning approach to predict the coke yield of commercial FCC unit. *Ind. Eng. Chem. Res.* **2022**, *61*, 8422–8431.
44. Zhang, M.X.; Yang, Z.; Zhao, Y.P.; et al. A hybrid safety monitoring framework for industrial FCC disengager coking rate based on FPM, CFD, and ML. *Process Saf. Environ.* **2023**, *175*, 17–33.
45. He, G.; Luo, L.; Zhou, L.; et al. Deep learning prediction of yields of fluid catalytic cracking via differential evolutionary dual-stage attention-based LSTM. *Fuel* **2024**, *370*, 131826.
46. Yue, Z.H.; Wang, Y.J.; Duan, J.Y.; et al. TS2Vec: Towards universal representation of time series. In Proceedings of the the Thirty-Sixth AAAI Conference on Artificial Intelligence, Virtual, 22 February–1 March 2022; pp 8980–8988.
47. Xu, R.Y.; Song, Z.R.; Wu, J.G.; et al. Change-point detection with deep learning: A review. *Front. Eng. Manag.* **2025**, *12*, 154–176.
48. Keshavarz, M.; Huang, B. Bayesian and expectation maximization methods for multivariate change point detection. *Comput. Chem. Eng.* **2014**, *60*, 339–353.
49. Liu, R.; Wang, H.; Yu, X.M. Shared-nearest-neighbor-based clustering by fast search and find of density peaks. *Inf. Sci.* **2018**, *450*, 200–226.
50. Zhang, X.; Qu, J.H. Density peaks clustering based on shared nearest neighbors and dense degree. In Proceedings of the 8th International Conference on Intelligent Computing and Signal Processing (ICSP), Xi'an, China, 21 – 23 April 2023; pp. 1088–1091.
51. Zou, T.G.; Zhou, M.W.; Wang, C.; et al. Pre-Shift fill control of wet clutches in heavy tracked vehicles using velocity prediction and a model predictive control framework. *Control Eng. Pract.* **2026**, *173*, 106950.
52. Yuan, X.F.; Huang, L.F.; Ye, L.J.; et al. Quality prediction modeling for industrial processes using multiscale attention-based convolutional neural network. *IEEE Trans. Cybern.* **2024**, *54*, 2696–2707.
53. Cui, D.S.; Qin, J.W.; He, F.; et al. MP3Net: Multi-scale patch parallel prediction networks for multivariate time series forecasting. In Proceedings of the International Joint Conference on Neural Networks (IJCNN), Yokohama, Japan, 30 June–5 July 2024; pp. 1–7.
54. Fang, Z.Y.; Gao, S.W.; Dang, X.C.; et al. Transformer enhanced by local perception self-attention for dynamic soft sensor modeling of industrial processes. *Meas. Sci. Technol.* **2024**, *35*, 055123.
55. Masoumi, M.; Sadrameli, S.; Towfighi, J.; et al. Simulation, optimization and control of a thermal cracking furnace. *Energy* **2006**, *31*, 516–527.